

## A Carbon Nanohorn–Porphyrin Supramolecular Assembly for Photoinduced Electron-Transfer Processes

María Vizuete,<sup>[a]</sup> María José Gómez-Escalonilla,<sup>[a]</sup> José Luis G. Fierro,<sup>[b]</sup>  
Atula S. D. Sandanayaka,<sup>[c]</sup> Taku Hasobe,<sup>\*,[c, d]</sup> Masako Yudasaka,<sup>\*,[e]</sup> Sumio Iijima,<sup>[e]</sup>  
Osamu Ito,<sup>\*,[f]</sup> and Fernando Langa<sup>\*,[a]</sup>

**Abstract:** A supramolecular assembly of zinc porphyrin–carbon nanohorns (CNHs) was constructed in a polar solvent. An ammonium cation was covalently connected to the CNH through a spacer (sp) (CNH-sp-NH<sub>3</sub><sup>+</sup>) and bound to a crown ether linked to a zinc porphyrin (Crown-ZnP). Nanohybrids CNH-sp-NH<sub>3</sub><sup>+</sup>;Crown-ZnP and CNH-sp-NH<sub>3</sub><sup>+</sup> were characterized by several techniques, such as high-resolution transmission electron microscopy, thermogravimetric analysis, X-ray photoelectron spectroscopy, and Raman spectroscopy. The photoinduced electron-transfer processes of the nanohybrids have been confirmed by using

time-resolved absorption and fluorescence measurements by combining the steady-state spectral data. Fluorescence quenching of the ZnP unit by CNH-sp-NH<sub>3</sub><sup>+</sup> has been observed, therefore, photoinduced charge separation through the excited singlet state of the ZnP unit is suggested for the hybrid material, CNH-sp-NH<sub>3</sub><sup>+</sup>;Crown-ZnP. As transient absorption spectral experiments reveal the formation of the radi-

cal cation of the ZnP unit, electron generation is suggested as a counterpart of the charge-separation on the CNHs; such an electron on the CNHs is further confirmed by migrating to the hexylviologen dication (HV<sup>2+</sup>). Accumulation of the electron captured from HV<sup>+</sup> is observed as electron pooling in solution in the presence of a hole-shifting reagent. Photovoltaic performance with moderate efficiency is confirmed for CNH-sp-NH<sub>3</sub><sup>+</sup>;Crown-ZnP deposited onto nanostructured SnO<sub>2</sub> films.

**Keywords:** carbon nanohorns · electron transfer · photovoltaic cells · porphyrinoids · supramolecular chemistry

[a] M. Vizuete, Dr. M. J. Gómez-Escalonilla, Prof. F. Langa  
Instituto de Nanociencia, Nanotecnología  
y Materiales Moleculares (INAMOL)  
Universidad de Castilla-La Mancha  
45071 Toledo (Spain)  
Fax: (+34) 925268840  
E-mail: Fernando.LPuente@uclm.es

[b] Prof. J. L. G. Fierro  
Instituto de Catálisis y Petroleoquímica, CSIC  
Cantoblanco, 28049, Madrid (Spain)

[c] Dr. A. S. D. Sandanayaka, Dr. T. Hasobe  
School of Materials Science  
Advanced Institute of Science and Technology  
Asahidai, Nomi, 923-1292 (Japan)

[d] Dr. T. Hasobe  
Department of Chemistry, Faculty of Science and Technology  
Keio University, Yokohama 223-8522 (Japan)  
PRESTO, JST, 4-1-8, Kawaguchi, Saitama, 332-0012 (Japan)  
E-mail: hasobe@keio.ac.jp

[e] Dr. M. Yudasaka, Prof. S. Iijima  
Nanotube Research Center  
National Institute of Advanced Industrial and Technology  
Higashi, Tsukuba, Ibaraki 305-8565 (Japan)  
E-mail: m-yudasaka@aist.go.jp

[f] Prof. O. Ito  
Institute of Multidisciplinary Research for Advanced Materials  
Tohoku University, Katahira, Sendai, 980-8577 (Japan)  
E-mail: ito@tagen.tohoku.ac.jp

 Supporting information for this article is available on the WWW under <http://dx.doi.org/10.1002/chem.201000299>.

## Introduction

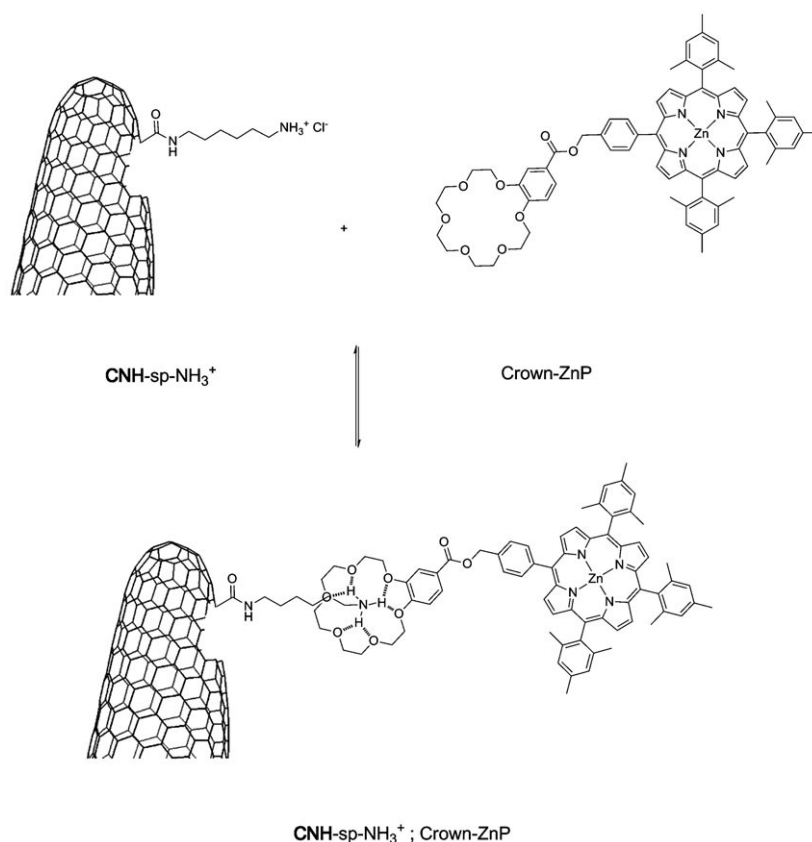
Carbon-based nanostructured materials have been extensively investigated for use in nanotechnological applications.<sup>[1]</sup> The most widely investigated all-carbon materials are fullerenes and carbon nanotubes.<sup>[1]</sup> Recently, carbon nanohorns (CNHs), which are single-graphene tubules with highly strained conical ends, have been synthesized and are intriguing materials.<sup>[2]</sup> In CNHs, horn-like structures are assembled to form dahlia-like spherical aggregates with diameters ranging between 50 and 100 nm.<sup>[2]</sup> One of the merits of CNHs is the high carbon purity due to the absence of any metal impurities, resulting from the synthetic procedure of using laser ablation methods on highly purified graphite without any metal catalysts.<sup>[2]</sup> Thus, CNHs have attracted a great deal of attention for various potential applications, such as gas storage, catalyst supports, drug carrier systems, and optoelectronic devices.<sup>[2]</sup>

To fabricate the CNHs on substrates, it is important to disperse CNHs in solution and thus obtain homogeneous CNH solutions, which then allows various precise studies with spectroscopic methods to be carried out on the solution state.<sup>[3]</sup> Besides the dispersion improvements, covalent and noncovalent attachments of various active compounds both onto the graphite-like side walls and at the conical-shaped tips, which only slightly perturb the  $\pi$ -electronic network of CNHs, have improved the wide applications of the dispersed CNHs. In this respect, Tagmatarchis and co-workers have succeeded in a number of chemical modifications of CNHs.<sup>[3]</sup>

To mimic natural photosynthesis, nanohybrids consisting of carbon-based materials and porphyrin pigments are particularly promising as artificial photosynthetic models,<sup>[4,5]</sup> in which the visible-light absorbing porphyrins act as light-harvesting antennae and high electron donors.<sup>[6,7]</sup> On the other hand, carbon-based materials, such as fullerenes and carbon nanotubes act as strong electron acceptors. Thus, the porphyrins form donor-acceptor nanohybrids with carbon nanomaterials, which function as photosynthetic reaction centers under light illumination.<sup>[4-7]</sup> It has also been reported that direct excitation of the nanocarbon materials with light also induces the charge separation,<sup>[8,9]</sup> thus, generated electrons on CNHs can be transferred to the electrodes

and the hole-shift reagents in the solution, which leads to photovoltaic cells.<sup>[8]</sup> Recently, it has been confirmed that photo-illumination of the chemically attached chromophores on CNHs induces efficient charge separation.<sup>[10]</sup> We also reported that the chemically modified CNHs are dispersible in organic solvents, when the attached chromophores are soluble in the solvents.<sup>[11-14]</sup> A few studies have reported the application of chemically modified CNHs in photovoltaic cells, with the porphyrins dispersible in solutions;<sup>[15]</sup> however, the maximum efficiency was relatively low compared with other nanocarbon structures.<sup>[8]</sup> Thus, it is necessary to modify the type of connection by using other porphyrins to improve the stabilization of the photoinduced charge-separated states to the extent that they persist for appropriately long times to mediate the electron-hole pair to the appropriate electrodes. Finally, we have constructed photovoltaic cells to obtain higher efficiencies.

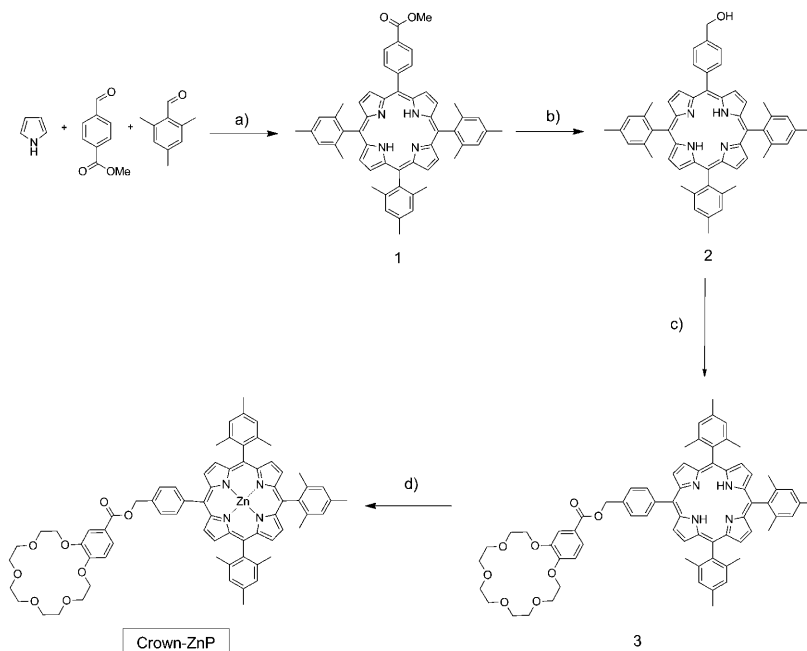
In the present study, we first synthesized the ammonium cation-connected CNH through a spacer (sp) (CNH-sp-NH<sub>3</sub><sup>+</sup>), which is dispersible homogeneously in polar solvents; therefore, CNH-sp-NH<sub>3</sub><sup>+</sup> has potential for various applications.<sup>[16]</sup> We further functionalized CNH-sp-NH<sub>3</sub><sup>+</sup> with a crown ether appended to a porphyrin (Crown-ZnP)<sup>[17]</sup> to produce an inclusion complex, CNH-sp-NH<sub>3</sub><sup>+</sup>;Crown-ZnP, (Scheme 1) to investigate the light-induced charge-separation processes in polar media.



Scheme 1. Formation of CNH-sp-NH<sub>3</sub><sup>+</sup>;Crown-ZnP.

## Results and Discussion

**Synthesis of Crown-ZnP:** Crown ether porphyrin (Crown-ZnP) was prepared according to the procedures shown in Scheme 2. The precursor porphyrin with a methyl ester



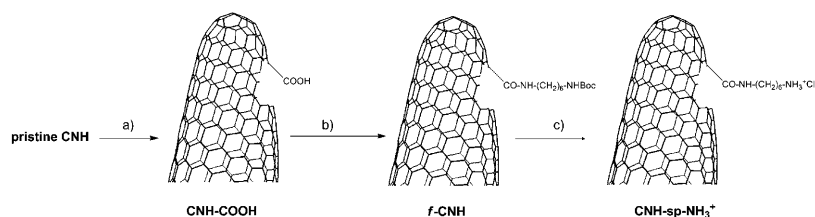
Scheme 2. Reagents and conditions: a)  $\text{BF}_3\text{OEt}_2$ ,  $\text{CHCl}_3$ , RT, 1 h; then DDQ, RT, 1 h,  $\text{EtN}_3$ , 16%; b)  $\text{LiAlH}_4$ , THF, RT, 12 h, 98%; c) 4'-(chlorocarbonyl)benzo[18]crown-6,  $\text{CH}_2\text{Cl}_2$ , pyridine, reflux, 4 days, 35%; d)  $\text{Zn}(\text{OAc})_2 \cdot 2\text{H}_2\text{O}$ ,  $\text{CHCl}_3$ , MeOH, reflux, 2 h, 49%.

group (**1**) was prepared in 16% yield by the Lindsey method<sup>[18]</sup> and the intermediate porphyrin with an alcohol group (**2**) was obtained in 98% yield by using a literature procedure.<sup>[19]</sup> Porphyrin with crown ether (**3**) was obtained in moderate yield (35%) by esterification of alcohol **2**<sup>[18]</sup> with 4'-(chlorocarbonyl)benzo[18]crown-6 in refluxing dichloromethane. Finally, the free-base porphyrin **3** was treated with zinc acetate to obtain the desired Crown-ZnP in 49% yield. All these compounds were characterized by  $^1\text{H}$  NMR and  $^{13}\text{C}$  NMR spectroscopy, and MALDI-TOF mass spectrometry (see the Supporting Information). Analysis of the  $^1\text{H}$  NMR spectra of Crown-ZnP revealed all the expected signals (see Figure S2 in the Supporting Information) including the [18]crown-6 entity hydrogen signals, which appear between  $\delta = 3.5$  and 4.5 ppm; the typical fingerprint of the porphyrin appears at  $\delta = 8.87$  and 8.75 ppm as two doublets and at  $\delta =$

8.70 as one broad singlet. Finally, the MALDI-TOF mass spectrometric analysis revealed the molecular ion peak of Crown-ZnP at  $m/z$  1171.3244 (calcd: 1170.44) (see Figure S4 in the Supporting Information).

**Preparation and characterization of  $\text{CNH-sp-NH}_3^+$ :** As shown in Scheme 3, the treatment of the  $\text{CNH-COOH}$  with *tert*-butyl-*N*-(6-aminoethyl) carbamate (*N*-Boc-1,6-diaminohexane; Boc = *tert*-butoxycarbonyl) in DMF afforded the protected *f*-CNH. Finally, the Boc protecting group of the *f*-CNH was easily cleaved upon treatment with HCl/dioxane (4M) yielding quantitatively the target  $\text{CNH-sp-NH}_3^+$ .

The target  $\text{CNH-sp-NH}_3^+$  was characterized by using various analytical and spectroscopic methods, all data being consistent with the proposed structure. Figure 1 shows the Raman spectrum of  $\text{CNH-sp-NH}_3^+$ , which reveals the presence of two prominent bands, one at  $\tilde{\nu} \approx 1350 \text{ cm}^{-1}$  (D-band) and one at  $\tilde{\nu} \approx 1590 \text{ cm}^{-1}$  (G-band). These bands are known to be characteristic of  $\text{CNHs}$ .<sup>[20]</sup> The D-band is attributed to defect sites, such as  $\text{sp}^3$  carbons, origi-



Scheme 3. Reagents and conditions: a)  $\text{H}_2\text{O}_2$ ; b)  $\text{NH}_2(\text{CH}_2)_6\text{NH-Boc}$ , DMF,  $50^\circ\text{C}$ , 5 days; c) HCl-dioxane (4M), 12 h.

nating from a one-phonon second-order process producing an elastic scattering<sup>[21]</sup> and is commonly used for monitoring the process of functionalization (change of C-atom hybridization from  $\text{sp}^2$  to  $\text{sp}^3$ ). An increase in the intensity of the D-band for  $\text{CNH-COOH}$  and  $\text{CNH-sp-NH}_3^+$ , as compared to that of the pristine  $\text{CNH}$ , was observed (Figure 1), which provides evidence of functionalization of these two materials. Furthermore, the additional increase of the D-band from  $\text{CNH-COOH}$  to  $\text{CNH-sp-NH}_3^+$  is attributed to the fur-

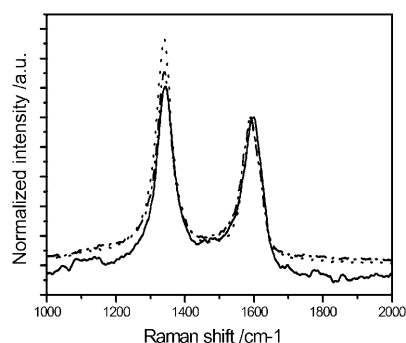


Figure 1. Raman spectra of pristine **CNH** (solid line), **CNH-COOH** (dash dotted line) and **CNH-sp-NH<sub>3</sub><sup>+</sup>** (dotted line) obtained by excitation at  $\lambda = 532$  nm. The spectra are normalized with the peak intensity of the G band at  $\lambda = 1550$   $\text{cm}^{-1}$ ; the peak height at  $\lambda = 1350$   $\text{cm}^{-1}$  increases in the order of pristine **CNH** (solid line), **CNH-COOH** (dash dotted line), and **CNH-sp-NH<sub>3</sub><sup>+</sup>** (dotted line).

ther functionalization (and additional  $\text{sp}^3$  carbon atoms) owing to the presence of the amide group, ethylene spacer, and  $-\text{NH}_3^+$ .

To further characterize **CNH-COOH** and **CNH-sp-NH<sub>3</sub><sup>+</sup>**, thermogravimetric analysis (TGA) was employed. In Figure 2, the obtained thermogram for **CNH-sp-NH<sub>3</sub><sup>+</sup>** is de-

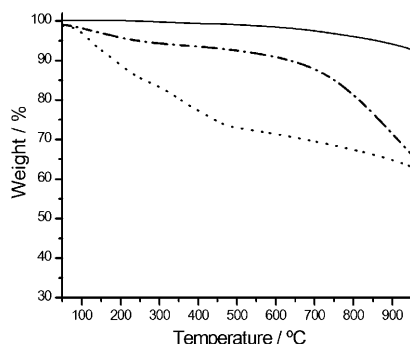


Figure 2. TGA curves recorded on raising the temperature at a rate of  $10^\circ\text{C min}^{-1}$  under  $\text{N}_2$  of pristine **CNH** (solid line), **CNH-COOH** (dash dotted line), and **CNH-sp-NH<sub>3</sub><sup>+</sup>** (dotted line).

icted and compared with that of **CNH-COOH** and pristine **CNH**. Pristine **CNH** is thermally stable under a  $\text{N}_2$  atmosphere up to  $800^\circ\text{C}$ ; **CNH-COOH** shows weight loss resulting from decarboxylation until  $700^\circ\text{C}$  by about 8% compared with the pristine **CNH**. The analysis of **CNH-sp-NH<sub>3</sub><sup>+</sup>** presents a higher weight loss of about 27% at  $550^\circ\text{C}$ , owing to the cleavage of the amide bond connecting the alkyl ammonium cation. These losses correspond to one functional group per  $\approx 40$  carbon atoms (6–7 benzene rings) of the **CNH** framework for both compounds. This result confirms that the attachment of the  $-\text{sp-NH}_3^+$  group occurs through the monoprotected diamine (*N*-Boc-1,6-diaminohexane) to **CNH-COOH** with the amide bonds, followed by the acid treatment.

X-ray photoelectron spectroscopy (XPS) provided clear additional evidence of the proposed structure of **CNH-sp-**

**NH<sub>3</sub><sup>+</sup>** by identifying and quantifying the functional groups anchored to the surface of **CNHs**.<sup>[22]</sup> The high-resolution C 1s, O 1s, N 1s, and Cl 2p core-level spectra of a sample of **CNH-sp-NH<sub>3</sub><sup>+</sup>** are displayed in Figure 3a–d, respectively.

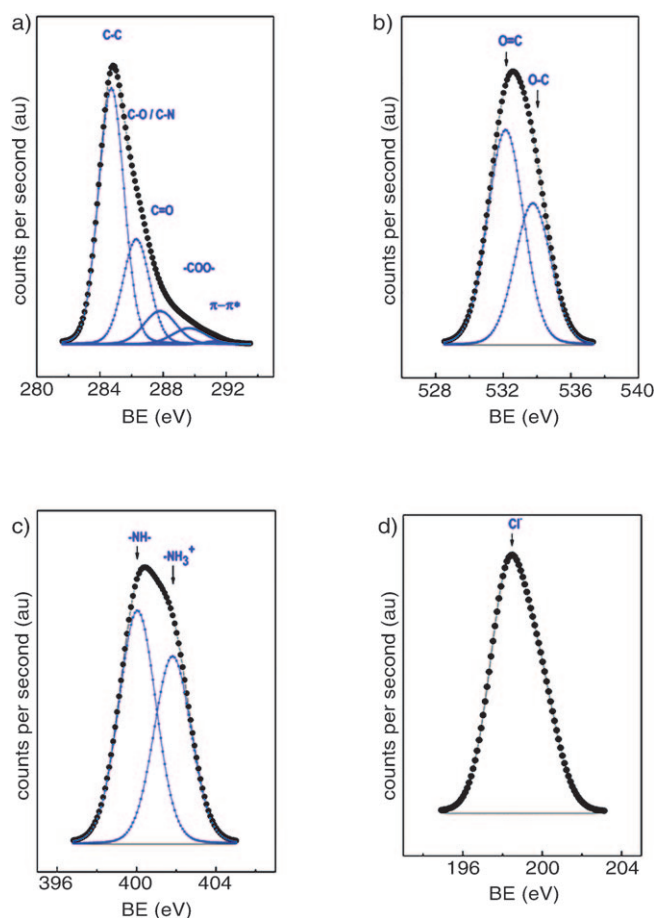


Figure 3. High-resolution core-level spectra of **CNH-sp-NH<sub>3</sub><sup>+</sup>Cl<sup>-</sup>**: a) C 1s, b) O 1s, c) N 1s, and d) Cl 2p.

The C 1s peak was satisfactorily curve-resolved with four components (Figure 3a) according to the peak assignment used by Stankovich et al.<sup>[23]</sup> The most intense peak at 284.4 eV is attributed to the  $\text{sp}^2$  C–C bonds of graphitic carbon. The component at 286.4 eV has been often assigned to C–OH (together with C–N and C–Cl bonds) and the components at 287.8 and 289.6 eV to C=O and  $-\text{COO}-$  species, respectively. A weak component at around 291.0 eV was observed and corresponds to a  $\pi \rightarrow \pi^*$  transition of the carbon atoms in graphene structures.<sup>[24]</sup> Similarly, the O 1s spectrum has been curve-resolved with two components (Figure 3b). A main component at 532.4 eV corresponds to O=C surface groups and a minor one at 533.9 eV is often associated with O–C bonds,<sup>[25]</sup> demonstrating the existence of oxygen functional groups on the graphene surface. The high-resolution N 1s spectrum (Figure 3c) displays two components, one at a binding energy of 400.2 eV, belonging to N atoms bonded to alkyl chains, and another at 401.8 eV of

similar intensity originating from the  $\text{-NH}_3^+$  moiety.<sup>[25]</sup> In addition, the Cl 2p core-level displayed the Cl 2p<sub>3/2</sub> component at 198.3 eV (Figure 3d) associated with the Cl<sup>-</sup> ion, which acts as counter anion for the  $\text{-NH}_3^+$  moiety (see Scheme 3).<sup>[25]</sup>

Among the atomic percentages derived from XPS (see the Supporting Information, Table S1), the C percentage is 85.7%, the remaining contributions are: O atoms 11.5%, N atoms 1.8%, and Cl atoms 1.0%. The Cl atom percentage, which is related to its presence as a counter ion of  $\text{-NH}_3^+$ , reveals that the  $\text{-NH}_3^+$  ion accounts for almost one half of the N content, as each  $\text{CNH-sp-NH}_3^+$  unit includes two kinds of N atoms (amide N and terminal  $\text{NH}_3^+$  in 1:1 ratio); thus, the ratio  $\text{NH}_3^+/\text{Cl}^- = 0.9$  fits fairly well with the theoretical value of 1, as expected from the formula in Scheme 3. Excess O atoms may result from unreacted  $\text{-COOH}$  and/or adsorbed  $\text{O}_2$ .

#### Preparation of the nanohybrid $\text{CNH-sp-NH}_3^+;\text{Crown-ZnP}$ :

By mixing Crown-ZnP with  $\text{CNH-sp-NH}_3^+$  in DMF at room temperature, the nanohybrid  $\text{CNH-sp-NH}_3^+;\text{Crown-ZnP}$  was readily prepared as a stable, homogeneous, black solution. The formation of  $\text{CNH-sp-NH}_3^+;\text{Crown-ZnP}$  was substantiated by several techniques, as shown in the following sections.

**HRTEM characterization of the nanohybrids:** The nanostructures of  $\text{CNH-sp-NH}_3^+;\text{Crown-ZnP}$  were observed by using high-resolution transmission electron microscopy (HRTEM). A typical image is shown in Figure 4 top, in which the dahlia-like structure is visible, meaning that the chemical treatments do not destruct much of the original dahlia-like structure. The existence of Zn atoms was clearly indicated in the EDX spectrum of  $\text{CNH-sp-NH}_3^+;\text{Crown-ZnP}$ , as shown in Figure 4 bottom, which corresponds to

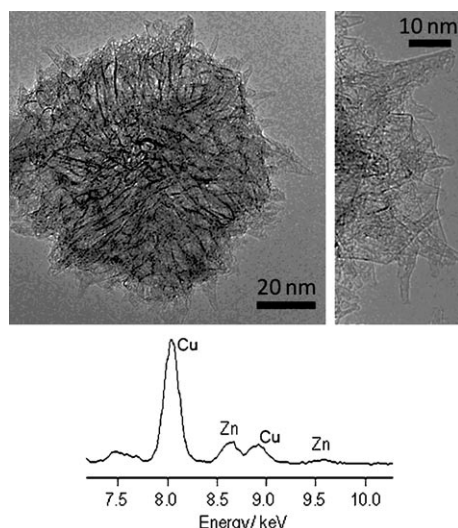


Figure 4. Top: HRTEM image of  $\text{CNH-sp-NH}_3^+;\text{Crown-ZnP}$  obtained from DMF solution. Bottom: EDX spectrum of  $\text{CNH-sp-NH}_3^+;\text{Crown-ZnP}$ ; Cu is due to the grid used for holding specimen.

blockages near the horns of  $\text{CNHs}$ , owing to small ZnP molecules (Figure 4 top right).

**Electrochemical characterization:** Cyclic voltammetric studies were performed to understand the redox behavior of the  $\text{CNH-sp-NH}_3^+;\text{Crown-ZnP}$  nanohybrid. Figure 5 shows the oxidation of Crown-ZnP with increasing amounts of  $\text{CNH-}$

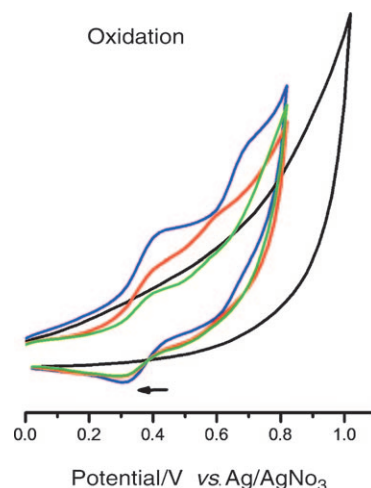


Figure 5. Cyclic voltammograms of Crown-ZnP (blue line) upon addition of increasing amounts of  $\text{CNH-sp-NH}_3^+$  (red to green line (final concentrations = Crown-ZnP ( $4.27 \times 10^{-7} \text{ M}$ ) and  $\text{CNH-sp-NH}_3^+$  (0.5 mg/100 mL; 1720  $\mu\text{L}$  in 2 mL)) containing 0.1 M  $(n\text{Bu})_4\text{NClO}_4$  in DMF. The black line corresponds to  $\text{CNH-sp-NH}_3^+$ . Scan rate:  $100 \text{ mV s}^{-1}$ .

$\text{sp-NH}_3^+$ . The first oxidation potential of Crown-ZnP was located at  $E_{1/2} = 0.37 \text{ V}$  versus  $\text{Ag/AgNO}_3$ , corresponding to the one-electron oxidation of the ZnP moiety. Addition of  $\text{CNH-sp-NH}_3^+$  resulted in a small cathodic shift of the oxidation wave ( $\approx 20 \text{ mV}$ ) of the Crown-ZnP moiety, owing to the interaction with  $\text{CNH}$  moieties,<sup>[17]</sup> which supports the fact that the high electron-donor ability of the ZnP moiety is retained even in the nanohybrids.

**Steady-state absorption spectroscopic characterization:** Absorption spectral changes of Crown-ZnP on addition of  $\text{CNH-sp-NH}_3^+$  in DMF solution are shown in Figure 6. The sharp absorption band at  $\lambda = 420 \text{ nm}$  is assigned to the Soret band of the ZnP unit. The intensity of the  $\lambda = 420 \text{ nm}$  band decreases on addition of  $\text{CNH-sp-NH}_3^+$ , with featureless bands in the UV-visible and near-IR regions, which is an additional piece of evidence for the formation of the inclusion complexes with Crown-ZnP.<sup>[17]</sup> Also, the presence of the isobestic points at  $\lambda = 420$  and  $433 \text{ nm}$  implies a predominant conversion from the Crown-ZnP to the  $\text{CNH-sp-NH}_3^+;\text{Crown-ZnP}$  nanohybrid (see Figure 6b).

**Steady-state fluorescence measurements:** With the excitation at  $\lambda = 433 \text{ nm}$  (one of the isobestic points) of the Crown-ZnP moiety in the nanohybrids, the fluorescence bands appeared at  $\lambda = 650$  and  $700 \text{ nm}$ , as shown in Figure 7.

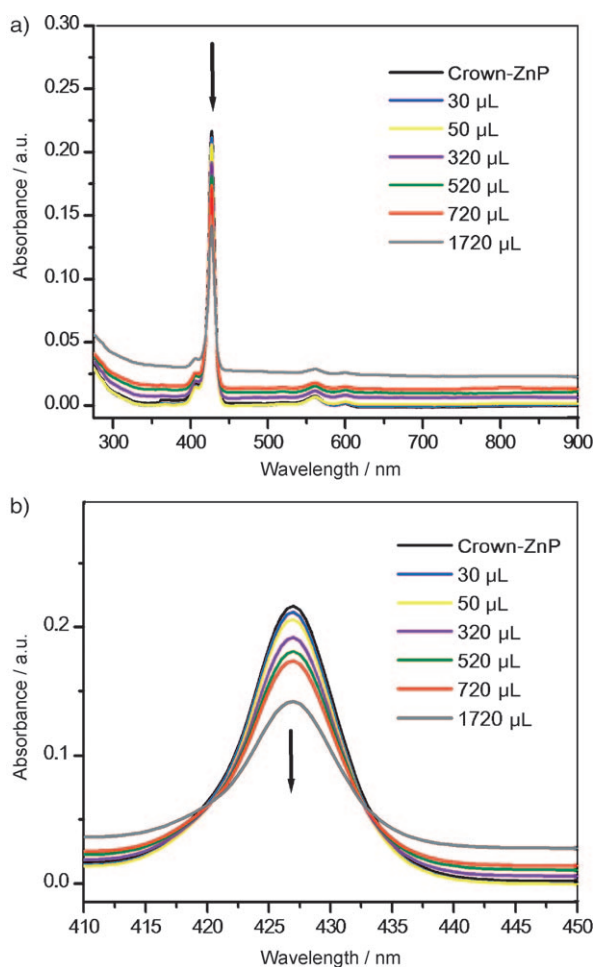


Figure 6. a) Absorption spectral changes of Crown–ZnP (black line;  $4.27 \times 10^{-7}$  M in DMF) on addition of increasing amounts of **CNH-sp-NH<sub>3</sub><sup>+</sup>** (concentration 0.5 mg/100 mL; from 30 to 1720 μL in 2 mL DMF). b) Spectra of wavelength expansion near Soret-band region, showing two isobestic points at  $\lambda = 420$  and 433 nm.

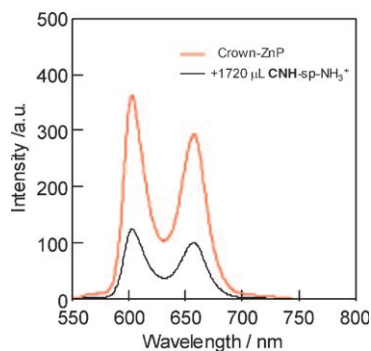


Figure 7. Fluorescence spectra of Crown–ZnP ( $4.27 \times 10^{-7}$  M; 2 mL) before and after addition of **CNH-sp-NH<sub>3</sub><sup>+</sup>** (0.5 mg/100 mL 1720 μL) in DMF;  $\lambda_{\text{ex}} = 433$  nm (isobestic point).

The fluorescence intensities of the Crown–ZnP moiety were quenched (67%) on addition of **CNH-sp-NH<sub>3</sub><sup>+</sup>** in DMF, which provides evidence for the formation of the nanohybrid structure of **CNH-sp-NH<sub>3</sub><sup>+</sup>;crown-ZnP**.<sup>[17]</sup> A control

experiment performed with the **CNH-sp-NH<sub>3</sub><sup>+</sup>** precursor (*f*-CNH, see Scheme 3) shows only slight quenching of the Crown–ZnP fluorescence (see Figure S5 in the Supporting Information). These results suggest that the intramolecular character of the quenching of the fluorescence is caused by the photophysical events in the excited singlet state of the Crown–ZnP moiety (<sup>1</sup>ZnP\*) in the vicinity of **CNHs**, such as a charge-separation process.<sup>[17]</sup>

**Fluorescence lifetime measurements:** The fluorescence time profiles of the Crown–ZnP moiety in the nanohybrid solution measured by using the excitation with picosecond pulsed-laser light at  $\lambda = 400$  nm and monitored by streakscope are shown in Figure 8, in which the shortening of the

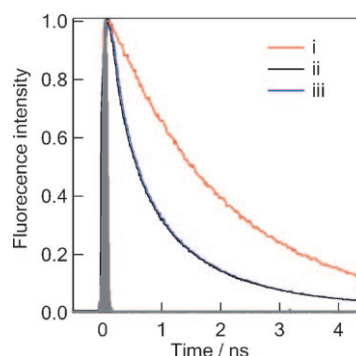


Figure 8. Fluorescence–time profiles in the  $\lambda = 600$ –700 nm region in DMF solution;  $\lambda_{\text{ex}} = 400$  nm. i) Crown–ZnP ( $4.27 \times 10^{-4}$  M; 4 mL), ii and iii) **CNH-sp-NH<sub>3</sub><sup>+</sup>;Crown–ZnP** nanohybrids ( $4.27 \times 10^{-4}$  M: 0.5 mg/100 mL = 3 mL:1 mL for (ii) and 2 mL:2 mL for (iii)).

fluorescence lifetime of the Crown–ZnP moiety was observed. The fluorescence lifetime shortening is almost maximum under similar concentrations of **CNH-sp-NH<sub>3</sub><sup>+</sup>** to the steady-state fluorescence quenching. From the curve-fittings with bi-exponential functions for both time profiles (ii) and (iii), the fluorescence lifetime ( $\tau_{\text{f}}^{\text{sample}}$ ) of the Crown–ZnP moiety was evaluated to be 370 ps (fraction = 40%) and 1200 ps (fraction = 60%), respectively, which are shorter than that of the unbound Crown–ZnP [ $\tau_{\text{f}}^{\text{ref}} = 2040$  ps (fraction = 100%)].

These observations indicate efficient quenching of the Crown-<sup>1</sup>ZnP\* moiety by **CNH-sp-NH<sub>3</sub><sup>+</sup>** in the nanohybrids. The shorter fluorescence lifetime in polar DMF can be attributed to the charge separation within the nanohybrids via the <sup>1</sup>ZnP\* moiety, generating **CNH<sup>-</sup>-sp-NH<sub>3</sub><sup>+</sup>;Crown–ZnP<sup>+</sup>**. The rate constant ( $k_{\text{CS}}^{\text{S}}$ ) and the quantum yield ( $\Phi_{\text{CS}}^{\text{S}}$ ) of the charge separation through the <sup>1</sup>ZnP\* moiety were evaluated from the shorter fluorescence component by the difference from that of the unbound Crown–ZnP.<sup>[26]</sup> The  $k_{\text{CS}}^{\text{S}}$  value was determined to be  $2.2 \times 10^9$  s<sup>-1</sup> and the  $\Phi_{\text{CS}}^{\text{S}}$  value was 0.81 (a total value was given as  $\Phi_{\text{CS}}^{\text{S}} \times \text{fraction} = 0.33$ ), suggesting a moderately efficient charge-separation process through the Crown-<sup>1</sup>ZnP\*. On the other hand, for the longer fluorescence lifetime a  $k_{\text{CS}}^{\text{S}}$  value of  $3.3 \times 10^8$  s<sup>-1</sup> was determined and the  $\Phi_{\text{CS}}^{\text{S}}$  value was 0.40 ( $\Phi_{\text{CS}}^{\text{S}} \times \text{frac}$

tion=0.24), which may be assigned to a slow charge-separation process for the relatively distant Crown-<sup>1</sup>ZnP\* moieties from the CNH surface. The total  $\Phi_{CS}^S$  evaluated from the fluorescence lifetimes is 0.57, which is in satisfactory agreement with the steady-state fluorescence quenching of 67%, supporting the reliability of both methods.

**Electron-mediating experiments:** To confirm the charge separation in the nanohybrids, steady-state absorption spectral measurements were performed by irradiation of the nanohybrids with light in the presence of hexyl viologen ( $HV^{2+}$ ), which is a well-known electron-mediating reagent. The accumulation of  $HV^{+}$  was confirmed by a characteristic band at  $\lambda = 620$  nm (Figure 9), resulting from the electron pooling to  $HV^{2+}$ , when a hole shifter such as 1-benzyl-1,4-dihydronicotinamide (BNAH) was added.<sup>[27]</sup>

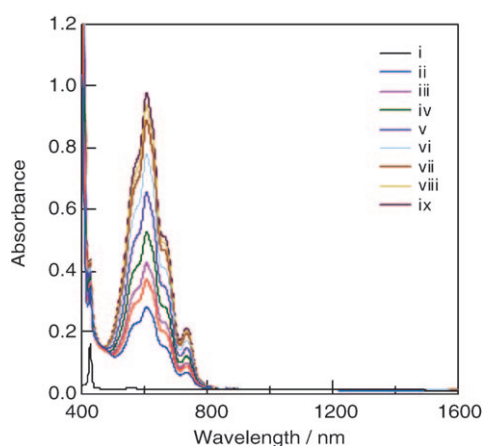


Figure 9. Steady-state absorption spectral changes observed after  $\lambda = 532$  nm laser light irradiation of  $CNH\text{-}sp\text{-}NH_3^+$ ;Crown-ZnP ( $4.27 \times 10^{-4}$  M: 0.5 mg/100 mL = 2 mL:2 mL) in the presence of  $HV^{2+}$  (0.1 mM) and BNAH. Each spectrum is the maximum one observed with repeated laser light irradiation. [BNAH] = i) 0, ii) 0.2, iii) 0.4, iv) 0.6, v) 0.8, vi) 1.0, vii) 1.2, viii) 1.4, and ix) 1.6 mM in Ar-saturated DMF (1.0 cm optical cell length; the  $\lambda = 532$  nm laser light has a 5 ns pulse width and  $\approx 3$  mJ/pulse power).

Each absorption spectrum exhibits the maximum value obtained after the repeated irradiation with  $\lambda = 532$  nm laser-light (usually 2–5 times of 5 ns pulsed laser light). From the observed absorbance at  $\lambda = 620$  nm, the maximum concentration of  $HV^{+}$  was found to be 0.08 mM, from which the conversion was evaluated to be 80% versus the feed of  $HV^{2+}$  (0.1 mM) in the presence of excess BNAH (1.6 mM). On the other hand, in the absence of BNAH, no absorption of  $HV^{+}$  was accumulated even after the laser-light irradiation of the nanohybrids. On increasing the BNAH concentration, amounts of  $HV^{+}$  increased, which indicates that back electron transfer from the electron-rich  $HV^{+}$  to the electron-poor  $ZnP^{+}$  is suppressed by the hole shift (HS) from  $ZnP^{+}$  to BNAH. After the hole shift, BNAH changes to  $BNAH^{+}$ , which irreversibly converts to 1-benzyl nicotinamide ( $BNA^+$ ), as a stable hole trap.

In a control experiment without  $CNH\text{-}sp\text{-}NH_3^+$ , such  $HV^{+}$  accumulation was not observed, although direct photoinduced electron transfer from Crown-<sup>1</sup>ZnP\* (or Crown-<sup>3</sup>ZnP\*) to  $HV^{2+}$  is possible, which indicates that  $CNH\text{-}sp\text{-}NH_3^+$  is indispensable for the accumulation of  $HV^{+}$ .

**Nano-second transient absorption spectra:** To investigate the transfer and migration mechanisms of electron and hole, the transient absorption spectra were recorded upon excitation of the Crown-ZnP moiety of the nanohybrids with  $\lambda = 532$  nm laser light after a nanosecond pulse duration (Figure 10). In the  $CNH\text{-}sp\text{-}NH_3^+$ ;Crown-ZnP nanohybrids,

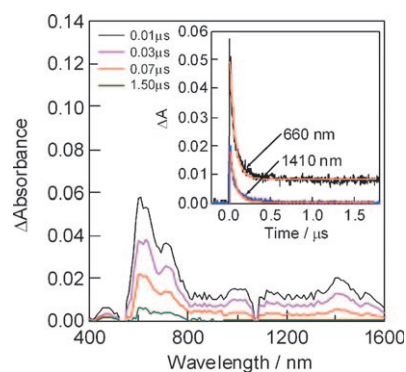


Figure 10. Nanosecond transient absorption spectra of  $CNH\text{-}sp\text{-}NH_3^+$ ; Crown-ZnP ( $4.27 \times 10^{-4}$  M : 0.5 mg/100 mL = 2 mL:2 mL) observed by  $\lambda = 532$  nm (5 ns pulse width and  $\approx 3$  mJ/pulse) laser irradiation in Ar-saturated DMF. Inset: Absorption-time profiles.

the observed transient absorption band in the  $\lambda = 600$ –800 nm region with a maximum at  $\lambda = 610$ –640 nm can be attributed to the Crown-ZnP<sup>+</sup> moiety.<sup>[6]</sup> The absorption bands in the near-IR region with a peak at  $\lambda = 1410$  nm can be considered as trapped electrons in the CNHs, as a counterpart to the Crown-ZnP<sup>+</sup> moiety, as similar broad absorption bands were observed for the trapped electrons in CNH (CNH<sup>-</sup>) in our previous papers.<sup>[11,12]</sup> The time profile at  $\lambda = 640$  nm shown in the inset of Figure 10 was curve-fitted by an exponential function, giving a first-order rate constant of  $1.2 \times 10^7$  s<sup>-1</sup> for the Crown-ZnP<sup>+</sup> moiety in Ar-saturated DMF. This rate constant can be attributed to the intra-nanohybrid charge recombination ( $k_{CR}$ ) within  $CNH\text{-}sp\text{-}NH_3^+$ ;Crown-ZnP<sup>+</sup>. In addition, the decay rate at  $\lambda = 1410$  nm is almost the same as that at  $\lambda = 640$  nm, supporting the fact that the  $\lambda = 1410$  nm absorption is due to CNH<sup>-</sup> as a counterpart of the Crown-ZnP<sup>+</sup> moiety. Thus, the lifetime of the radical ion pair (RIP),  $\tau_{RIP}$ , of  $CNH\text{-}sp\text{-}NH_3^+$ ; Crown-ZnP<sup>+</sup> was evaluated to be 85 ns from the value of  $k_{CR}$ . In the inset of Figure 10, although complete decay was observed at  $\lambda = 1410$  nm, the slow decay part was observed at  $\lambda = 640$  nm after 200 ns, which may be attributed to surviving Crown-ZnP<sup>+</sup> after the fate of CNH<sup>-</sup>-sp-NH<sub>3</sub><sup>+</sup> due to the encounter of an electron with defects in CNH.

If both BNAH and  $HV^{2+}$  were added to the nanohybrid solutions, the transient absorption bands in the near-IR region almost disappeared within 100 ns (Figure 11). In-

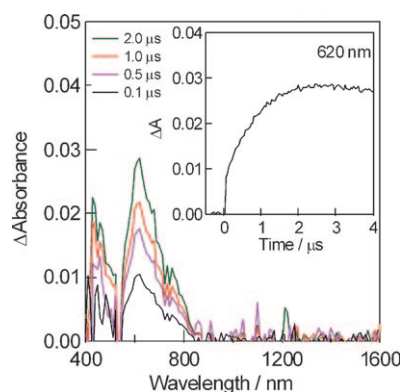


Figure 11. Nanosecond transient absorption spectra of Crown–ZnP with 1720 mL of  $CNH\text{-}sp\text{-}NH_3^+$  ( $4.27 \times 10^{-4}$  M: 0.5 mg/100 mL = 2 mL:2 mL) in the presence of  $HV^{2+}$  (0.1 mM) and BNAH (1.6 mM) observed by  $\lambda = 532$  nm ( $\approx 3$  mJ/pulse) laser-light irradiation in Ar-saturated DMF. Inset: Absorption–time profiles.

stead, the increasing absorption was observed in the  $\lambda = 600\text{--}800$  nm region with a peak at  $\lambda = 620$  nm. Although the absorption peak position is similar to the that of Crown–ZnP $^{2+}$ , quite different time profiles suggest that the  $\lambda = 620$  nm band in the presence of  $HV^{2+}$  is ascribed to the  $HV^{+}$  absorption band. Thus, Figure 11 indicates that the  $HV^{+}$  absorption band appeared at  $\lambda = 620$  nm with complete annihilation of  $CNH\text{-}sp\text{-}NH_3^+$  at  $\lambda = 1410$  nm, suggesting that an electron-mediating process from  $CNH\text{-}sp\text{-}NH_3^+$  to  $HV^{2+}$  takes place generating  $HV^{+}$ , as an electron pool in solution. On the other hand, the absorption band of the Crown–ZnP $^{2+}$  moiety was completely consumed by the hole shift to BNAH.

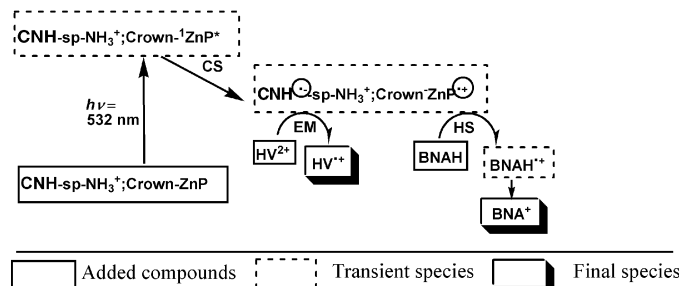
The rise of  $HV^{+}$  at  $\lambda = 620$  nm in the inset of Figure 11 may correspond to the intermolecular electron-mediating process from  $CNH\text{-}sp\text{-}NH_3^+$  to  $HV^{2+}$  within 200 ns ( $k_{\text{rise}}^{\text{fast}} = 5 \times 10^6$  s $^{-1}$ ), almost coinciding with the decay of  $CNH\text{-}sp\text{-}NH_3^+$  at  $\lambda = 1410$  nm. Taking the  $HV^{2+}$  concentration into consideration, the bimolecular rate constant for the apparent  $HV^{+}$  accumulation process was calculated to be  $k_{\text{EM}} = 10^{10}$  M $^{-1}$  s $^{-1}$ , which is close to the diffusion-controlled limit ( $k_{\text{Diff}} = 5 \times 10^9$  M $^{-1}$  s $^{-1}$  in DMF).<sup>[28]</sup>

If BNAH is also present, the formed absorption band of  $HV^{+}$  at  $\lambda = 620$  nm persists without decay after 2–3  $\mu$ s as shown in the inset of Figure 11, indicating that back electron transfer from electron-rich  $HV^{+}$  to Crown–ZnP $^{2+}$  was almost suppressed by the excess BNAH, owing to the consumption of Crown–ZnP $^{2+}$  supporting the hole shift from the Crown–ZnP $^{2+}$  to BNAH.<sup>[28]</sup>

On addition of only  $HV^{2+}$  to nanohybrids, the transient spectra showed a decrease of the near-IR bands (see Figure S6 in the Supporting Information), accompanied by the rapid decay of the  $\lambda = 1410$  nm band, confirming the elec-

tron-mediating process from  $CNH\text{-}sp\text{-}NH_3^+$  to  $HV^{2+}$ .<sup>[11,12]</sup> The most prominent difference is the shorter lifetime of the generated  $HV^{+}$  (less than 200 ns), suggesting that the back electron transfer from the Crown–ZnP $^{2+}$  to  $HV^{+}$  is working to consume  $HV^{+}$ .

**Electron transfer scheme:** These observations, induced by the illumination of nanohybrids with light, can be explained by the processes summarized in Scheme 4, in which charge



Scheme 4. Schematic representation for the photoinduced electron transfer processes of the nanohybrid  $CNH\text{-}sp\text{-}NH_3^+$ ;Crown–ZnP.

separation initially takes place through the  $^1ZnP^*$  moiety, generating  $CNH\text{-}sp\text{-}NH_3^+$ ;Crown–ZnP $^{2+}$  in DMF solution. On addition of  $HV^{2+}$  and BNAH, the electron on  $CNH$  mediates to  $HV^{2+}$ , leading to an accumulation of  $HV^{+}$ . From the one-electron oxidation ( $\approx 0.4$  V) and the lowest singlet excited-state energy (2.0 eV) of the ZnP, the charge-separation process becomes exothermic, if the reduction potential of  $CNH$  is less negative than  $-1.6$  V versus  $Ag/AgNO_3$ , which is reasonably negative enough to be compatible with the reported reduction potential of single-walled carbon nanotubes (SWCNT) of  $-0.6$  V.<sup>[12]</sup> The intermolecular electron-mediating (EM) and hole-shifting (HS) processes with additives are also exothermic processes or almost isoenergetic processes.

**Photovoltaic cells:** To construct the photovoltaic cells, the drop-cast method was applied to fabricate films of  $CNH\text{-}sp\text{-}NH_3^+$ ;Crown–ZnP onto an OTE/SnO $_2$  electrode. The absorption spectrum of OTE/SnO $_2$ /CNH-sp-NH $_3^+$ ;Crown–ZnP (Figure 12a) exhibits the Soret band and Q-band, whereas OTE/SnO $_2$ /CNH-sp-NH $_3^+$  shows a featureless broad band in the visible region (Figure 12b). Compared with the absorption spectra in Figure 6, broadening of the absorption bands of OTE/SnO $_2$ /CNH-sp-NH $_3^+$ ;Crown–ZnP was observed, suggesting the aggregations of the Crown–ZnP moieties in the films.

Photoelectrochemical measurements were performed in a three-compartment cell equipped with a potentiostat, OTE/SnO $_2$ /CNH-sp-NH $_3^+$ ;Crown–ZnP or OTE/SnO $_2$ /CNH-sp-NH $_3^+$  as a working electrode, and Pt wire as a counter electrode.<sup>[29,30]</sup> The  $I$ – $V$  characteristics of the OTE/SnO $_2$ /CNH-sp-NH $_3^+$ ;Crown–ZnP electrode under the illumination with white light are shown in Figure 13; the photocurrent density

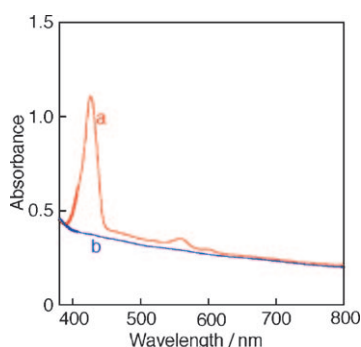


Figure 12. Steady-state absorption spectra of a) OTE/SnO<sub>2</sub>/CNH-sp-NH<sub>3</sub><sup>+</sup>;Crown-ZnP film and b) OTE/SnO<sub>2</sub>/CNH-sp-NH<sub>3</sub><sup>+</sup> film.

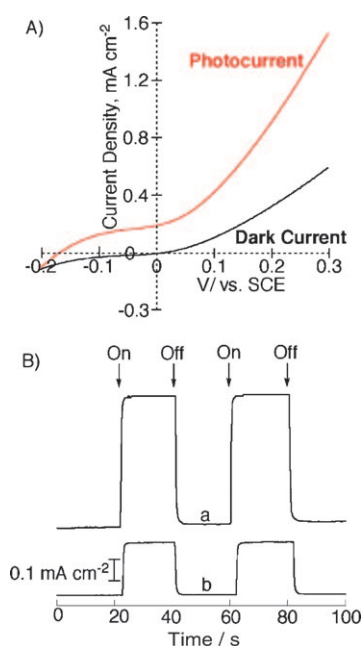


Figure 13. A) *I*-*V* characteristics of the OTE/SnO<sub>2</sub>/CNH-sp-NH<sub>3</sub><sup>+</sup>; Crown-ZnP electrode under illumination with white light (red curve; AM 1.5 condition; input power = 100 mW cm<sup>-2</sup>) and in the dark (black curve). B) Photocurrent generation responses of a) OTE/SnO<sub>2</sub>/CNH-sp-NH<sub>3</sub><sup>+</sup>;Crown-ZnP and b) OTE/SnO<sub>2</sub>/CNH-sp-NH<sub>3</sub><sup>+</sup> at an applied bias voltage of 0.2 V versus SCE. Electrolyte: LiI 0.5 M, I<sub>2</sub> 0.01 M in acetonitrile; input power = 100 mW cm<sup>-2</sup>.

increases compared with the dark current. The photocurrent density increases with an electrochemical bias, suggesting increased charge separation and the facile transport of charge carriers in the OTE/SnO<sub>2</sub>/CNH-sp-NH<sub>3</sub><sup>+</sup>;Crown-ZnP electrode under a positive bias potential. Importantly, the photocurrent generation density of the electrode can be controlled by using the three-compartment cell (Figure 13), in which the net photocurrent generation density of the OTE/SnO<sub>2</sub>/CNH-sp-NH<sub>3</sub><sup>+</sup>;Crown-ZnP electrode at +0.2 V ( $\approx 0.58 \text{ mA cm}^{-2}$ ) was higher than the case at 0 V ( $\approx 0.23 \text{ mA cm}^{-2}$ ).

In Figure 13a, photocurrent responses of the OTE/SnO<sub>2</sub>/CNH-sp-NH<sub>3</sub><sup>+</sup>;Crown-ZnP electrode (response A) and OTE/SnO<sub>2</sub>/CNH-sp-NH<sub>3</sub><sup>+</sup> electrode (response B) under the white light illumination are performed by applying bias potential (0.2 V vs. SCE). Both photocurrent responses are prompt, steady, and reproducible during repeated on/off cycles of the light illumination. The short circuit photocurrent densities ( $I_{sc}$ ) at applied bias potentials of 0.2 V versus SCE are about  $0.40 \text{ mA cm}^{-2}$  for the OTE/SnO<sub>2</sub>/CNH-sp-NH<sub>3</sub><sup>+</sup>;Crown-ZnP electrode (see response A) and  $0.15 \text{ mA cm}^{-2}$  for the OTE/SnO<sub>2</sub>/CNH-sp-NH<sub>3</sub><sup>+</sup> electrode (see response B). This indicates that the OTE/SnO<sub>2</sub>/CNH-sp-NH<sub>3</sub><sup>+</sup>;Crown-ZnP electrode is superior to the OTE/SnO<sub>2</sub>/CNH-sp-NH<sub>3</sub><sup>+</sup> one. The photocurrent action spectra of the OTE/SnO<sub>2</sub>/CNH-sp-NH<sub>3</sub><sup>+</sup>;Crown-ZnP electrode, OTE/SnO<sub>2</sub>/CNH-sp-NH<sub>3</sub><sup>+</sup> electrode, and OTE/SnO<sub>2</sub>/Crown-ZnP electrode were measured by examining the wavelength dependence of the incident photon-to-current conversion efficiency (IPCE). The IPCE values are calculated by normalizing the photocurrent densities for incident light energy and intensity using of the expression given in Equation (1),<sup>[31]</sup>

$$\text{IPCE (\%)} = 100 \times 1240 \times i / (W_{in} \times \lambda_{ex}) \quad (1)$$

in which,  $i$  is the photocurrent density ( $\text{A cm}^{-2}$ ),  $W_{in}$  is the incident-light intensity ( $\text{W cm}^{-2}$ ), and  $\lambda_{ex}$  is the excitation wavelength (in nm). The photocurrent action spectra were recorded by using the standard three-compartment cell under an applied bias potential of 0.2 V versus SCE. As shown in Figure 14, the photocurrent action spectrum of

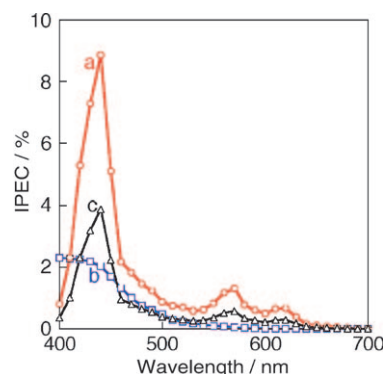


Figure 14. Photocurrent action spectra of IPCE; a) OTE/SnO<sub>2</sub>/CNH-sp-NH<sub>3</sub><sup>+</sup>;Crown-ZnP electrode, b) OTE/SnO<sub>2</sub>/CNH-sp-NH<sub>3</sub><sup>+</sup> electrode, and c) OTE/SnO<sub>2</sub>/Crown-ZnP electrode at an applied bias potential of 0.2 V versus SCE. Electrolyte: LiI 0.5 M, I<sub>2</sub> 0.01 M in acetonitrile.

IPCE for OTE/SnO<sub>2</sub>/CNH-sp-NH<sub>3</sub><sup>+</sup>;Crown-ZnP electrode follows the same pattern as the absorption spectrum in Figure 12a; furthermore, the maximum value of IPCE reaches 9% at  $\lambda = 450 \text{ nm}$ , which is 4.5 times larger than that of the OTE/SnO<sub>2</sub>/CNH-sp-NH<sub>3</sub><sup>+</sup> electrode (2% in  $\lambda = 400\text{--}450 \text{ nm}$

region) and 2.2 times larger than that of the OTE/SnO<sub>2</sub>/Crown–ZnP electrode (4% at 450 nm).

The maximum IPCE value (9%) obtained for the OTE/SnO<sub>2</sub>/CNH-sp-NH<sub>3</sub><sup>+</sup>;Crown–ZnP electrode, is comparable to that for the covalently grafted porphyrin to CNHs.<sup>[15]</sup> Even by the comparison with the covalently linked porphyrin to the single-walled carbon nanotubes, the obtained IPCE value for CNH-sp-NH<sub>3</sub><sup>+</sup>;Crown–ZnP is comparable or better.<sup>[32,33]</sup> These results clearly demonstrate that photo-induced ET processes in the CNH-sp-NH<sub>3</sub><sup>+</sup>;Crown–ZnP hybrid possesses the light-energy conversion ability (vide infra), supporting considerably high potentials for application to photovoltaic devices.

## Conclusion

We have prepared a new supramolecular assembly of CNH and a zinc-porphyrin (CNH-sp-NH<sub>3</sub><sup>+</sup>;Crown–ZnP) for light-sensitive nanohybrids by relatively simple self-assembly procedures. By the excitation of the nanohybrids, the generation of the unique charge-separated state, CNH<sup>•-</sup>-sp-NH<sub>3</sub><sup>+</sup>;Crown–ZnP<sup>+</sup> via the excited singlet state of the Crown–ZnP moiety was confirmed. As ZnP<sup>•+</sup> and CNH<sup>•-</sup> persist longer than 100 ns, they have enough time to mediate the electron on CNH to HV<sup>2+</sup> to concomitantly shift to the hole of ZnP to BNAH under appropriate concentration ranges. Thus, accumulation of HV<sup>•+</sup> was observed by irradiation of the nanohybrids in light in the presence of a sacrificial hole shifter, BNAH, as summarized in Scheme 4, in which the ET mechanisms are confirmed with the transient absorption and time-resolved fluorescence measurements. Usually, the accumulated HV<sup>•+</sup> can be further used as an electron source transferring to catalysts for H<sub>2</sub> evolution in aqueous solution. Additionally, photoelectrochemical cells of the CNH-sp-NH<sub>3</sub><sup>+</sup>;Crown–ZnP hybrid materials were fabricated onto OTE/SnO<sub>2</sub> electrodes. The OTE/SnO<sub>2</sub>/CNH-sp-NH<sub>3</sub><sup>+</sup>;Crown–ZnP electrode exhibited a maximum IPCE of 9%. Based on these experiments, we conclude that organization of molecular assemblies achieved with the CNH-sp-NH<sub>3</sub><sup>+</sup>;Crown–ZnP hybrid materials is a key factor in attaining improved light-energy conversion properties.

## Experimental Section

**Chemicals:** CNHs were produced by CO<sub>2</sub> laser ablation of graphite in the absence of any metal catalyst under an Ar atmosphere (760 Torr) at room temperature; the purity of CNHs was as high as 90% with less amorphous carbons. Then, the CNHs were treated with H<sub>2</sub>O<sub>2</sub>, which generated the corresponding carboxylic acid groups in CNH-COOH. All other chemicals utilized in the synthesis and spectroscopic measurements were purchased from Aldrich Chemicals (Milwaukee, WI) and were used as received. Tetrabutylammonium perchlorate, *n*Bu<sub>4</sub>NClO<sub>4</sub>, used in the electrochemical studies, was obtained from Fluka Chemicals.

**Synthesis of Crown-H<sub>2</sub>P, 3 (see Scheme 2):** A solution of 4-carboxybenzo[18]crown-6 (200 mg, 0.56 mmol), SOCl<sub>2</sub> (408 μL, 5.6 mmol), and pyridine (1 mL) in dry CH<sub>2</sub>Cl<sub>2</sub> (30 mL) was refluxed under argon gas for 3 h. After the mixture was cooled, the solvent was evaporated and the crude

residue was washed several times with boiling petroleum ether. Then, the solvent was evaporated and the resultant colorless solid was redissolved in dry CH<sub>2</sub>Cl<sub>2</sub> (20 mL). Then, pyridine (1 mL) was added followed by porphyrin **2**<sup>[9]</sup> (see Scheme 2, 50 mg, 0.05 mmol). The reaction mixture was refluxed under an argon atmosphere for four days. The solvent was evaporated, and the crude product was purified by column chromatography (silica gel, CH<sub>2</sub>Cl<sub>2</sub> followed by CH<sub>2</sub>Cl<sub>2</sub>/CH<sub>3</sub>OH 90:10). Evaporation of the solvents yielded the desired free-base porphyrin crown-H<sub>2</sub>P compound **3** as a purple solid (19 mg, 35%); <sup>1</sup>H NMR (400 MHz, CDCl<sub>3</sub>) δ = 8.81 (d, 2H, β-pyrrole H, *J* = 4.58 Hz), 8.70 (d, 2H, β-pyrrole H, *J* = 4.58 Hz), 8.65 (s, 4H, β-pyrrole H), 8.23 (d, 2H, phenyl H, *J* = 7.78 Hz), 7.89 (dd, 1H, benzocrown phenyl H, *J* = 8.44 Hz, *J* = 1.60 Hz), 7.81 (d, 2H, phenyl H, *J* = 7.78 Hz), 7.74 (d, 1H, benzocrown phenyl H, *J* = 1.60 Hz), 7.29 (s, 6H), 6.96 (d, 1H, benzocrown phenyl H, *J* = 8.44 Hz), 5.71 (s, 2H), 4.34–4.20 (m, 4H, crown ethylene H), 4.05–3.95 (m, 4H, crown ethylene H), 3.85–3.66 (m, 12H, crown ethylene H), 2.64 (s, 9H), 1.86 (s, 18H), –2.54 ppm (br s, 2H, -NH); MS (MALDI-TOF, dithranol): *m/z*: 1109.6 [*M*+1].

**Synthesis of Crown–ZnP:** Crown-H<sub>2</sub>P **3** (16 mg, 0.014 mmol) was dissolved in CHCl<sub>3</sub> (10 mL), saturated zinc acetate in methanol was added, and the resulting mixture was refluxed for 2 h. Then, the reaction mixture was washed with water and dried over anhydrous Na<sub>2</sub>SO<sub>4</sub>. The crude Crown–ZnP solid was purified by washing several times with chloroform–pentane to give pure Crown–ZnP (8 mg, 49%); <sup>1</sup>H NMR (CDCl<sub>3</sub>, 400 MHz) δ = 8.87 (d, 2H, β-pyrrole H, *J* = 4.64 Hz), 8.75 (d, 2H, β-pyrrole H, *J* = 4.64 Hz), 8.70 (br s, 4H, β-pyrrole H), 8.24 (d, 2H, phenyl H, *J* = 7.92 Hz), 7.88 (dd, 1H, benzocrown phenyl H, *J* = 8.48 Hz, *J* = 1.60 Hz), 7.80 (d, 2H, phenyl H, *J* = 7.92 Hz), 7.73 (d, 1H, benzocrown phenyl H, *J* = 1.60 Hz), 7.27 (s, 6H), 6.95 (d, 1H, benzocrown phenyl H, *J* = 8.48 Hz), 5.70 (s, 2H), 4.30–4.21 (m, 4H, crown ethylene H), 4.00–3.92 (m, 4H, crown ethylene H), 3.81–3.68 (m, 12H, crown ethylene H), 2.63 (s, 9H); 1.85 ppm (s, 18H); <sup>13</sup>C NMR (CDCl<sub>3</sub>, 100 MHz) δ = 166.4, 149.9, 149.8, 149.7, 142.8, 139.2, 139.0, 138.9, 137.3, 135.3, 134.5, 132.0, 131.1, 131.0, 130.6, 127.6, 126.1, 125.5, 124.2, 122.8, 119.4, 118.8, 118.5, 117.9, 114.5, 112.2, 70.9, 70.7, 69.3, 66.5, 21.7, 21.6, 21.4 ppm; UV/Vis (DMF): λ<sub>max</sub> (log ε): 600 (3.1), 561 (3.5), 427(5.0), 405 nm (3.9); MS (MALDI-TOF, dithranol): *m/z*: 1171.3244 [*M*+1].

**Synthesis of CNH-sp-NH<sub>3</sub><sup>+</sup> (see Scheme 3):** CNH-COOH (50 mg) was suspended in DMF (100 mL) and the resulting mixture was sonicated for 5 min. *N*-Boc-1,6-diaminohexane was added (Boc = *tert*-butoxycarbonyl, 150 mg, 0.6 mmol) and the mixture was stirred at 50°C for five days to obtain *f*-CNH (Scheme 3), which was recovered by vacuum filtration over a Millipore membrane (PTFE, 0.1 μm), extensively washed with DMF, CH<sub>2</sub>Cl<sub>2</sub>, and Et<sub>2</sub>O, and dried under high vacuum. To produce CNH-sp-NH<sub>3</sub><sup>+</sup>, the Boc protecting group was removed by adding a solution of HCl–dioxane (4M; 20 mL) in a round-bottom flask, which was cooled by an ice-water bath under an argon atmosphere. After the mixture had been stirred overnight, it was filtered on a Millipore membrane (PTFE, 0.1 μm), followed by addition of fresh CH<sub>2</sub>Cl<sub>2</sub> with sonication, filtration through a 0.1 μm PTFE membrane and finally washing the solid material with EtOH. The collected black solid of CNH-sp-NH<sub>3</sub><sup>+</sup> was finally dried under high vacuum (54 mg). The FT-IR spectrum of CNH-sp-NH<sub>3</sub><sup>+</sup> exhibits the C–H stretching vibration modes of the alkyl chains around  $\tilde{\nu}$  = 2916 and 2850 cm<sup>-1</sup>, and a broad band around  $\tilde{\nu}$  = 3400 cm<sup>-1</sup> corresponding to the cationic ammonium group. Additionally, the covalent amide bonds are proven by the presence of carbonyl vibrations at  $\tilde{\nu}$  = 1637 cm<sup>-1</sup> (see Figure S7 in the Supporting Information).

**Formation of CNH-sp-NH<sub>3</sub><sup>+</sup>;Crown–ZnP:** crown–ZnP (4.27 × 10<sup>-7</sup> M in 2 mL DMF) and CNH-sp-NH<sub>3</sub><sup>+</sup> (concentration 0.5 mg/100 mL in DMF) were stirred for 2 min at room temperature.

**Preparation of OTE/SnO<sub>2</sub>/CNH-sp-NH<sub>3</sub><sup>+</sup>;Crown–ZnP films:** The desired volume of the CNH-sp-NH<sub>3</sub><sup>+</sup>;Crown–ZnP suspension (≈ 1 mL) was simply deposited onto an OTE/SnO<sub>2</sub> electrode by using the drop-cast method. The OTE/SnO<sub>2</sub> electrodes (with a surface area of 0.5 × 0.5 cm) coated with CNH-sp-NH<sub>3</sub><sup>+</sup>;Crown–ZnP gave the OTE/SnO<sub>2</sub>/CNH-sp-NH<sub>3</sub><sup>+</sup>;Crown–ZnP electrode. As reference electrodes, OTE/SnO<sub>2</sub>/CNH-sp-NH<sub>3</sub><sup>+</sup> and OTE/SnO<sub>2</sub>/Crown–ZnP were prepared similarly.

## Acknowledgements

Financial support from the Ministry of Science and Innovation of Spain, FEDER funds (Project CTQ2007-63363/PPQ and Consolider project HOPECS2007-00007) and the Fund from Junta de Comunidades de Castilla-La Mancha (Project PCI08-038) is gratefully acknowledged. The authors appreciate the JSPS for the support of Dr. A. S. D. Sandanayaka. We thank M. Irie, Dr. M. Nakamura, and Dr. M. Zhang for performing the TM and XDS experiments, and Dr. T. Azami and Dr. D. Kasuya for the preparing CNH. We also thank M. J. de la Mata for carrying out the TGA experiments. This work was partially supported by Grant-in-Aids for Scientific Research (No. 21710104 to T.H.) and special coordination funds for promoting science and technology from the Ministry of Education, Culture, Sports, Science and Technology, Japan.

- [1] a) P. M. Ajayan, *Chem. Rev.* **1999**, *99*, 1787–1800; b) S. Prabhpreet, S. Campidelli, S. Giordani, D. Bonifazi, A. Bianco, M. Prato, *Chem. Soc. Rev.* **2009**, *38*, 2214–2230; c) M. S. Dresselhaus, G. Dresselhaus, P. Avouris, *Carbon Nanotubes: Synthesis Structure, Properties and Applications*, Springer, Heidelberg, **2001**; d) S. Reich, C. Thomsen, J. Maultzsch, *Carbon Nanotubes: Basic Concepts and Physical Properties*, Wiley-VCH, Weinheim, **2004**; e) M. Meyyappan, *Carbon Nanotubes: Science and Applications*, CRC Press, New York, **2005**.
- [2] a) S. Iijima, M. Yudasaka, R. Yamada, S. Bandow, K. Suenaga, F. Kokai, K. Takahashi, *Chem. Phys. Lett.* **1999**, *309*, 165–170; b) S. Iijima, *Physica B+C* **2002**, *23*, 1–5; c) J. Fan, M. Yudasaka, Y. Kasuya, D. Kasuya, S. Iijima, *Chem. Phys. Lett.* **2004**, *397*, 5–10; d) K. Murata, A. Hashimoto, M. Yudasaka, D. Kasuya, K. Kaneko, S. Iijima, *Adv. Mater.* **2004**, *16*, 1520–1522; e) H. Murakami, K. Ajima, J. Miyawaki, M. Yudasaka, S. Iijima, K. Shiba, *Mol. Pharm.* **2004**, *1*, 399–405.
- [3] a) N. Tagmatarchis, A. Maigne, M. Yudasaka, S. Iijima, *Small* **2006**, *2*, 490–494; b) G. Pagona, J. Fan, N. Tagmatarchis, M. Yudasaka, S. Iijima, *Chem. Mater.* **2006**, *18*, 3918–3920.
- [4] For porphyrins noncovalently attached to carbon nanotubes, see: a) Y.-P. Sun, K. Fu, Y. Lin, W. Huang, *Acc. Chem. Res.* **2002**, *35*, 1096–1104; b) H. Kataura, Y. Maniwa, M. Abe, A. Fujiwara, K. Kikuchi, H. Imahori, Y. Misaki, S. Suzuki, Y. Achiba, *Appl. Phys. A* **2002**, *74*, 349–354; c) Y. Lin, B. Zhou, K. A. S. Fernando, P. Liu, L. F. Allard, Y.-P. Sun, *Macromolecules* **2003**, *36*, 7199–7204; d) H. Murakami, T. Nomura, N. Nakashima, *Chem. Phys. Lett.* **2003**, *378*, 481–485; e) M. C. Paiva, B. Zhou, K. A. S. Fernando, Y. Lin, J. M. Kennedy, Y.-P. Sun, *Carbon* **2004**, *42*, 2849–2854; f) S. Barazzouk, S. Hotchandani, K. Vinodgopal, P. V. Kamat, *J. Phys. Chem. B* **2004**, *108*, 17015–17018; g) Y. Lin, B. Zhou, Y. Lin, L. Gu, W. Wang, K. A. S. Fernando, K. Kumar, L. F. Allard, Y.-P. Sun, *J. Am. Chem. Soc.* **2004**, *126*, 1014–1015; h) I. Robel, B. A. Bunker, P. V. Kamat, *Adv. Mater.* **2005**, *17*, 2458–2463; i) D. M. Guldi, H. Taieb, G. M. A. Rahman, N. Tagmatarchis, M. Prato, *Adv. Mater.* **2005**, *17*, 871–875; j) A. Satake, Y. Miyajima, Y. Kobuke, *Chem. Mater.* **2005**, *17*, 716–724; k) J. Chen, C. P. Vollier, *J. Phys. Chem. B* **2005**, *109*, 7605–7609; l) G. M. A. Rahman, D. M. Guldi, S. Campidelli, M. Prato, *J. Mater. Chem.* **2006**, *16*, 62–65; m) M. Alvaro, P. Atienzar, P. de La Cruz, J. L. Delgado, V. Troiani, H. Garcia, F. Langa, A. Palkar, L. Echegoyen, *J. Am. Chem. Soc.* **2006**, *128*, 6626–6635; n) F. Cheng, S. Zhang, A. Adronov, L. Echegoyen, F. Diederich, *Chem. Eur. J.* **2006**, *12*, 6062–6070; o) K. Schulte, J. C. Swarbric, N. A. Smith, F. Bondino, E. Magnano, A. K. Khlobystov, *Adv. Mater.* **2007**, *19*, 3312–3316.
- [5] For porphyrins covalently attached to carbon nanotubes, see: a) H. Li, R. B. Martin, B. A. Harruff, R. A. Carino, Y.-P. Sun, *Adv. Mater.* **2004**, *16*, 896–900; b) D. Baskaran, J. W. Mays, X. P. Zhang, M. S. Bratcher, *J. Am. Chem. Soc.* **2005**, *127*, 6916–6917; c) Z. Guo, F. Du, D. Ren, Y. Chen, J. Zheng, Z. Liu, J. Tian, *J. Mater. Chem.* **2006**, *16*, 3021–3030; d) B. Ballesteros, G. de La Torre, C. Ehli, G. M. Aminur-Rahman, F. Agulló-Rueda, D. M. Guldi, T. Torres, *J. Am. Chem. Soc.* **2007**, *129*, 5061–5068.
- [6] a) H. Imahori, Y. Sakata, *Adv. Mater.* **1997**, *9*, 537–546; b) D. M. Guldi, M. Prato, *Acc. Chem. Res.* **2000**, *33*, 695–703; c) M. E. El-Khouly, O. Ito, P. M. Smith, F. D'Souza, *J. Photochem. Photobiol. C* **2004**, *5*, 79–104; d) H. Imahori, S. Fukuzumi, *Adv. Funct. Mater.* **2004**, *14*, 525–536; e) F. D'Souza, O. Ito, *Coord. Chem. Rev.* **2005**, *249*, 1410–1422.
- [7] R. Chitta, A. S. D. Sandanayaka, A. L. Schumacher, L. D'Souza, Y. Araki, O. Ito, F. D'Souza, *J. Phys. Chem. C* **2007**, *111*, 6947–6955.
- [8] a) T. Hasobe, S. Fukuzumi, P. V. Kamat, *Angew. Chem.* **2006**, *118*, 769–773; *Angew. Chem. Int. Ed.* **2006**, *45*, 755–759; b) T. Hasobe, S. Fukuzumi, P. V. Kamat, *J. Am. Chem. Soc.* **2005**, *127*, 11884–11885; c) T. Hasobe, *Phys. Chem. Chem. Phys.* **2010**, *12*, 44–57.
- [9] a) A. S. D. Sandanayaka, Y. Takaguchi, T. Uchida, Y. Sako, Y. Morimoto, Y. Araki, O. Ito, *Chem. Lett.* **2006**, *35*, 1188–1189; b) A. S. D. Sandanayaka, H. Orisaka, T. Kyotani, Y. Araki, O. Ito, *Carbon* **2007**, *45*, 684–687.
- [10] C. Cioffi, S. Campidelli, C. Sooambar, M. Marcaccio, G. Marcolongo, M. S. Meneghetti, D. Paolucci, F. Paolucci, C. Ehli, A. Rahman, M. G. V. Sgobba, D. M. Guldi, M. Prato, *J. Am. Chem. Soc.* **2007**, *129*, 3938–3945.
- [11] a) A. S. D. Sandanayaka, G. Pagona, N. Tagmatarchis, M. Yudasaka, S. Iijima, Y. Araki, O. Ito, *J. Mater. Chem.* **2007**, *17*, 2540–2546; b) G. Pagona, A. S. D. Sandanayaka, Y. Araki, J. Fan, N. Tagmatarchis, G. Charalambidis, P. Trohopoulos, A. G. Coutsolelos, B. Boitrel, M. Yudasaka, S. Iijima, O. Ito, *Adv. Funct. Mater.* **2007**, *17*, 1705–1711.
- [12] For carbon nanohorns, see: a) G. Pagona, A. S. D. Sandanayaka, Y. Araki, J. Fan, N. Tagmatarchis, M. Yudasaka, S. Iijima, O. Ito, *J. Phys. Chem. B* **2006**, *110*, 20729–20732; b) G. Pagona, A. S. D. Sandanayaka, A. Maigné, J. Fan, G. C. Papavassiliou, I. D. Petsalakis, B. R. Steele, M. Yudasaka, S. Iijima, N. Tagmatarchis, O. Ito, *Chem. Eur. J.* **2007**, *13*, 7600–7607; c) M. Zhang, M. Yudasaka, T. Murakami, K. Ajima, A. S. D. Sandanayaka, O. Ito, K. Tsuchita, S. Iijima, *Proc. Natl. Acad. Sci. USA* **2008**, *105*, 14773–14778; d) A. S. D. Sandanayaka, O. Ito, M. Zhang, K. Ajima, S. Iijima, M. Yudasaka, T. Murakami, K. Tsuchita, *Adv. Mater.* **2009**, *21*, 4366–4371.
- [13] a) P. Keller, A. Moradpour, *J. Am. Chem. Soc.* **1980**, *102*, 7193–7196; b) P. Keller, A. Moradpour, E. Amouyel, H. Kagan, *J. Mol. Catal.* **1980**, *7*, 539–542; c) A. I. Krasna, *J. Photochem. Photobiol. A* **1980**, *31*, 75–82; d) J. M. Calvert, T. J. Manuccia, R. J. Nowak, *J. Electrochem. Soc.* **1986**, *133*, 951–953; e) R. J. McMahon, R. K. Force, H. H. Patterson, M. S. Wrighton, *J. Am. Chem. Soc.* **1988**, *110*, 2670–2672; f) *Photosensitization of Porphyrins and Phthalocyanines* (Ed.: I. Okura), Gordon and Breach Science Publishers, Amsterdam, **2001**.
- [14] P. M. S. Monk, *The Viologens*, Wiley, New York, **1998**.
- [15] G. Pagona, A. S. D. Sandanayaka, T. Hasobe, G. Charalambidis, A. G. Coutsolelos, M. Yudasaka, S. Iijima, N. Tagmatarchis, *J. Phys. Chem. C* **2008**, *112*, 15735–15741.
- [16] a) R. Yuge, M. Yudasaka, J. Miyawaki, Y. Kubo, T. Ichihashi, H. Imai, E. Nakamura, H. Isobe, H. Yorimitsu, S. Iijima, *J. Phys. Chem. B* **2005**, *109*, 17861–17867; b) J. Miyawaki, M. Yudasaka, H. Imai, H. Yorimitsu, H. Isobe, E. Nakamura, S. Iijima, *J. Phys. Chem. B* **2006**, *110*, 5179–5181; c) H. Isobe, T. Tanaka, R. Maeda, E. Noiri, N. Solin, M. Yudasaka, S. Iijima, E. Nakamura, *Angew. Chem.* **2006**, *118*, 6828–6832; *Angew. Chem. Int. Ed.* **2006**, *45*, 6676–6680; d) A. S. D. Sandanayaka, O. Ito, T. Tanaka, H. Isobe, E. Nakamura, M. Yudasaka, S. Iijima, *New J. Chem.* **2009**, *33*, 2261–2266.
- [17] a) F. D'Souza, R. Chitta, S. Gadde, M. E. Zandler, A. S. D. Sandanayaka, Y. Araki, O. Ito, *Chem. Commun.* **2005**, 1279–1281; b) F. D'Souza, R. Chitta, A. S. D. Sandanayaka, N. K. Subbaiyan, L. D'Souza, Y. Araki, O. Ito, *Chem. Eur. J.* **2007**, *13*, 8277–8284; c) F. D'Souza, O. Ito, *Chem. Commun.* **2009**, 4913–4928.
- [18] J. S. Lindsey, S. Prathapan, T. E. Johnson, R. W. Wagner, *Tetrahedron* **1994**, *50*, 8941–8968.
- [19] A. A. Yasseri, D. Syomin, R. S. Loewe, J. S. Lindsey, F. Zaera, D. F. Bocian, *J. Am. Chem. Soc.* **2004**, *126*, 15603–15612.
- [20] T. Yamaguchi, S. Bandow, S. Iijima, *Chem. Phys. Lett.* **2004**, *389*, 181–185.

- [21] S. Utsumi, H. Honda, Y. Hattori, H. Kanoh, K. Takahashi, H. Sakai, M. Abe, M. Yudasaka, S. Iijima, K. Kaneko, *J. Phys. Chem. C* **2007**, *111*, 5572–5575.
- [22] S. Giordani, J.-F. Colomer, F. Cattaruzza, J. Alfonsi, M. Meneghetti, M. Prato, D. Bonifazi, *Carbon* **2009**, *47*, 578–588.
- [23] S. Stankovich, D. A. Dikin, R. D. Piner, K. A. Kohlhaas, A. Kleinhammes, Y. Jia, Y. Wu, S. T. Nguyen, R. S. Ruoff, *Carbon* **2007**, *45*, 1558–1565.
- [24] E. Bekyarova, M. E. Itkis, P. Ramesh, C. Berger, M. Sprinkle, W. A. de Heer, R. C. Haddon, *J. Am. Chem. Soc.* **2009**, *131*, 1336–1337.
- [25] M. J. Gómez-Escalonilla, P. Atienzar, J. L. G. Fierro, H. García, F. Langa, *J. Mater. Chem.* **2008**, *18*, 1592–1600, and references therein.
- [26]  $k_{CS} = (1/\tau_t)_{\text{sample}} - (1/\tau_t)_{\text{ref}}$  and  $\Phi_{CS} = [(1/\tau_t)_{\text{sample}} - (1/\tau_t)_{\text{ref}}] / (1/\tau)_{\text{sample}}$ ;  $(\tau_t)_{\text{ref}} = 2040$  ns.
- [27] a) S. Fukuzumi, S. Koumitsu, K. Hironaka, T. Tanaka, *J. Am. Chem. Soc.* **1987**, *109*, 305–316; b) S. Fukuzumi, H. Imahori, K. Okamoto, H. Yamada, M. Fujitsuka, O. Ito, D. M. Guldi, *J. Phys. Chem. A* **2002**, *106*, 1903–1908.
- [28] The first-order rate constant for the intermolecular electron transfer ( $k_{\text{first order}}$ ) as fast as a diffusion-controlled limit ( $k_{\text{Diff}}$ ) in the presence of  $[MV^{2+}] = 0.5$  mM can be evaluated as  $k_{\text{first order}} = k_{\text{Diff}} [MV^{2+}] = 5 \times 10^9 \text{ M}^{-1} \text{ s}^{-1} \times 5 \times 10^{-4} \text{ M}^{-1} = 2.5 \times 10^6 \text{ s}^{-1}$ , which is in good agreement with the  $HV^{++}$  rise rate ( $5 \times 10^6 \text{ s}^{-1}$ ). For the  $k_{\text{Diff}}$  value, see: S. I. Murov, I. Carmichael, G. L. Hug, *Handbook of Photochemistry*, Marcel-Dekker, New York, **1993**.
- [29] H. J. Lee, J. H. Yum, H. C. Leventis, S. M. Zakeeruddin, S. A. Haque, P. Chen, S. I. Seok, M. Grätzel, M. K. Nazeeruddin, *J. Phys. Chem. C* **2008**, *112*, 11600–11608.
- [30] Y. Ueno, H. Minoura, T. Nishikawa, M. Tsuiki, *J. Electrochem. Soc.* **1983**, *130*, 43–47.
- [31] T. Hasobe, Y. Kashiwagi, M. A. Absalom, J. Sly, K. Hosomizu, M. J. Crossley, H. Imahori, P. V. Kamat, S. Fukuzumi, *Adv. Mater.* **2004**, *16*, 975–979.
- [32] T. Hasobe, S. Fukuzumi, P. V. Kamat, *J. Phys. Chem. B* **2006**, *110*, 25477–25484.
- [33] T. Umeyama, M. Fujita, N. Tezuka, N. Kadota, Y. Matano, K. Yoshida, S. Isoda, H. Imahori, *J. Phys. Chem. C* **2007**, *111*, 11484–11493.

Received: February 3, 2010

Published online: August 4, 2010